Coherent Spin Pumping in a Strongly Coupled Magnon-Magnon Hybrid System

Yi Li,[1,2] Wei Cao,[3] Vivek P. Amin,[4,5] Zhizhi Zhang,[2,6] Jonathan Gibbons,[2] Joseph Sklenar,[7] John Pearson,[2] Paul M. Haney,[5] Mark D. Stiles,[5] William E. Bailey,[3,*] Valentine Novosad,[2] Axel Hoffmann,[2,‡] and Wei Zhang[1,2,†]

[1]*Department of Physics, Oakland University, Rochester, Michigan 48309, USA*
[2]*Materials Science Division, Argonne National Laboratory, Argonne, Illinois 60439, USA*
[3]*Materials Science and Engineering, Department of Applied Physics and Applied Mathematics, Columbia University, New York, New York 10027, USA*
[4]*Maryland Nanocenter, University of Maryland, College Park, Maryland 20742, USA*
[5]*Physical Measurement Laboratory, National Institute of Standards and Technology, Gaithersburg, Maryland 20899, USA*
[6]*School of Optical and Electronic Information, Huazhong University of Science and Technology, Wuhan 430074, China*
[7]*Department of Physics and Astronomy, Wayne State University, Detroit, Michigan 48202, USA*

We experimentally identify coherent spin pumping in the magnon-magnon hybrid modes of yttrium iron garnet/permalloy (YIG/Py) bilayers. By reducing the YIG and Py thicknesses, the strong interfacial exchange coupling leads to large avoided crossings between the uniform mode of Py and the spin wave modes of YIG enabling accurate determination of modification of the linewidths due to the dampinglike torque. We identify additional linewidth suppression and enhancement for the in-phase and out-of-phase hybrid modes, respectively, which can be interpreted as concerted dampinglike torque from spin pumping. Furthermore, varying the Py thickness shows that both the fieldlike and dampinglike couplings vary like $1/\sqrt{t_{Py}}$, verifying the prediction by the coupled Landau-Lifshitz equations.

Coherent phenomena have recently become an emerging topic for information processing with their success in quantum computing [1,2]. In spintronics, exchange-induced magnetic excitations, called spin waves, or magnons [3,4], are good candidates for coherent information processing where information can be encoded by both the amplitude and the phase of spin waves. For example, the interference of coherent spin waves can be engineered for spin wave logic operations [5–7], the coherent interaction of spin-torque oscillators leads to mutual synchronization [8–13], which can be applied in artificial neural networks [14,15]. and the coherent coupling between magnons and microwave cavities [16–23] opens up new opportunities for magnon-based quantum information science [24,25].

Recently, strong coupling between two magnonic systems has enabled excitations of forbidden spin wave modes [26–28] and high group velocity of propagating spin waves [29,30]. The coupling is dominated by the exchange interaction at the interface of the magnetic bilayers, providing a new pathway to coherently transfer magnon excitations between two magnetic systems possessing distinctive properties: from conductor to insulator, from uniform to nonuniform mode, and from high-damping to low-damping systems. However, the underlying physical mechanisms of the coupling are still not fully understood. First, what are the key parameters that dictate the coupling efficiency and enable one to reach the strong-coupling regime? Second, with the interfacial exchange coupling

acting as a fieldlike torque, is there a dampinglike torque associated with spin pumping [31–34]? To resolve both questions, large separations of the two hybrid modes are required in order to quantitatively analyze the coupling mechanism. The second question is also important for optimizing the coherence of spin wave transfer in hybrid systems. Furthermore, the parasitic effect on the incoherent spin current from the conduction band is absent [35–37] when using magnetic insulators such as yttrium iron garnet ($Y_3Fe_5O_{12}$, YIG) [30,38,39], which facilitates the study of spin pumping coherency.

In this work, we study YIG/permalloy ($Ni_{80}Fe_{20}$, Py) bilayers. By using much thinner YIG and Py films than studied in previous works [26,28], we achieve an exchange-induced separation of the two hybrid modes much larger than their linewidths, allowing us to study the evolution of their linewidths in the strong-coupling regime. We find a pronounced suppression of the total linewidth for the in-phase hybrid modes and a linewidth enhancement for the out-of-phase hybrid modes. The linewidths can be understood from the Landau-Lifshitz-Gilbert (LLG) equation with interfacial exchange coupling and mutual spin pumping, which provide the fieldlike and dampinglike interlayer coupling torques, respectively. Furthermore, the thickness dependence of the two coupling strengths agrees with the modeling of coupled LLG equations with mutual spin pumping. The sign of the fieldlike torque also reconfirms that the YIG and Py are coupled antiferromagnetically [26]. Our results provide important insights for improving the

coupling strength and coherence in magnon-magnon hybrid systems and pave the way for coherent information processing with exchange-coupled magnetic heterostructures.

The samples consist of YIG(100 nm)/Py(t_{Py}) bilayers where t_{Py} varies from 5 to 60 nm. YIG(100 nm) films were deposited by magnetron sputtering from a YIG target onto $Gd_3Ga_5O_{12}(111)$ substrates and annealed in air at 850 °C for 3 h to reach low-damping characteristics [40]. Before the deposition of Py films on top of YIG, the YIG surfaces were ion milled *in situ* for 1 min in order to enable good exchange coupling between Py and YIG [41]. For each Py thickness, one additional reference Py film was deposited on a Si/SiO_2 substrate during the same deposition.

The hybrid magnon dynamics were characterized by broadband ferromagnetic resonance with field modulation on a coplanar waveguide [Fig. 1(a)]. An in-plane magnetic field H_B saturates both the YIG and Py magnetizations. Their Kittel modes, which describe spatially uniform magnetization precession, are formulated as $\omega^2/\gamma^2 = \mu_0^2 H_r(H_r + M_s)$, where ω is the mode frequency, $\gamma/2\pi = (g_{eff}/2) \times 27.99$ GHz/T is the gyromagnetic ratio, H_r is the resonance

field, and M_s is the magnetization [42]. For YIG, the spatially nonuniform perpendicular standing spin wave (PSSW) modes can also be measured. An effective exchange field H_{ex} will lower the resonance field by $\mu_0 H_{ex}(k) = (2A_{ex}/M_s)k^2$, where A_{ex} is the exchange stiffness, $k = n\pi/t$, n labels the index of PSSW modes, and t is the film thickness [43].

Figure 1(b) shows the line shapes of the resonance fields for the first three resonance modes of YIG ($n = 0, 1, 2$) and the Py uniform mode ($n = 0$) measured for $t_{Py} = 9$ nm. For illustration, the YIG ($n = 0$) resonance is shifted to zero field. An avoided crossing is clearly observed when the Py uniform mode is degenerate with the YIG ($n = 2$) mode. This is due to the exchange coupling at the YIG/Py interface [26–28] providing a fieldlike coupling torque. Both in-phase and out-of-phase YIG/Py hybrid modes are strongly excited because the energy of the Py uniform mode is coherently transferred to the YIG PSSW modes through the interface [26]. The full-range frequency dependencies of the extracted resonance fields are plotted in Fig. 1(c). To analyze the two hybrid modes, we analyze our results with two independent Lorentzians because it facilitates a transparent physical picture and the fit line shapes agree well with our measurements. The mode crossing happens at $\omega_c/2\pi = 9.4$ GHz (black dashed line), which corresponds to the minimal resonance separation of the two hybrid modes. Fitting to the Kittel equation, we extract $\mu_0 M_s^{YIG} = 0.21$ T, $\mu_0 M_s^{Py} = 0.86$ T. From the exchange field offset as shown in Fig. 1(b), an exchange stiffness $A_{ex} = 2.6$ pJ/m is calculated for YIG, which is similar to previous reports [44].

The avoided crossing can be fitted to a phenomenological model of two coupled harmonic oscillators, as previously shown in magnon polaritons [16–18,20]:

$$\mu_0 H_c^{\pm} = \mu_0 \frac{H_r^{YIG} + H_r^{Py}}{2} \pm \sqrt{\left(\mu_0 \frac{H_r^{YIG} - H_r^{Py}}{2}\right)^2 + g_c^2}, \quad (1)$$

where $H_r^{YIG(Py)}$ is the resonance field of YIG (Py) and g_c is the interfacial exchange coupling strength. H_r^{YIG} and H_r^{Py} are both functions of frequency and are equal at ω_c. Note that for in-plane biasing field, the resonance field is nonlinear to the excitation frequency. This nonlinearity will be accounted for in the analytical reproduction of Eq. (1). The fitting yields $g_c = 8.4$ mT for $t_{Py} = 9$ nm.

Next, we focus on the linewidths of the YIG-Py hybrid modes. Figure 2(a) shows the line shape of the two hybrid modes for $t_{Py} = 7.5$ nm at $\omega_c/2\pi = 9.4$ GHz (same value as for 9-nm Py). These two eigenmodes correspond to the in-phase and out-of-phase magnetization precession of Py and YIG with the same weight, so they should yield the same total intrinsic damping. Nevertheless, a significant linewidth difference is observed, with the extracted full width at half maximum linewidth $\mu_0 \Delta H_{1/2}$ varying from 3.5 mT for the lower field resonance to 8.0 mT for the higher field resonance. Figure 2(b) shows
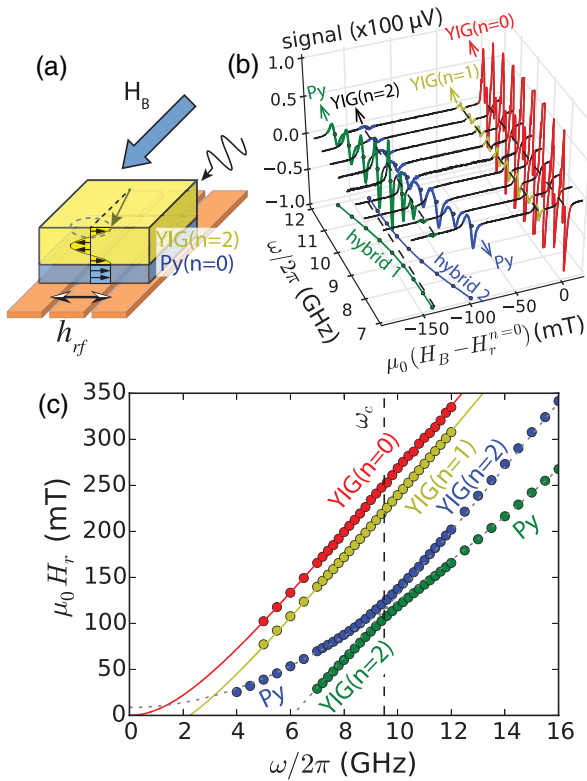

FIG. 1. (a) Illustration of the magnetization excitations in the YIG/Py bilayer with a coplanar waveguide. (b) Line shapes of the YIG(100 nm)/Py(9 nm) sample for the first three resonance modes of YIG and the uniform mode of Py. The field axis is shifted so that the resonance field of the YIG($n = 0$) mode is zero. (c) Unshifted evolution of the four modes in (b). Curves show the fits as uncoupled modes. The vertical dashed line denotes where the YIG($n = 2$) and Py($n = 0$) modes cross on the frequency axis at $\omega_c/2\pi = 9.4$ GHz.

the full-range evolution of the linewidth. Compared with the dotted lines which are the linear extrapolations of the YIG ($n = 2$) and Py linewidths, the linewidth of the higher-field hybrid mode (blue circles) exceeds the Py linewidth and the linewidth of the lower-field hybrid mode (green circles) reduces below the YIG linewidth when the frequency is near ω_c. This is the central result of this Letter. It suggests a coherent dampinglike torque which acts along or against the intrinsic damping torque depending on the phase difference of the coupled dynamics of YIG and Py, the same as the fieldlike torque acting along or against the Larmor precession. The dominant mechanism for the dampinglike torque is the spin pumping from the concerted dynamics of YIG and Py [31,32].

Because spin pumping is dissipative, we determine the mode with a broader (narrower) linewidth as the out-of-phase (in-phase) precession mode. In Fig. 2(a) the broader-linewidth mode exhibits a higher resonance field than the narrower-linewidth mode. This is a signature of antiferromagnetic exchange coupling at the YIG/Py interface [26]. From the resonance analysis we also find that all the SiO_2/Py samples show lower resonance fields than the Py samples grown on YIG [45], which agrees with the antiferromagnetic nature of the YIG/Py interfacial coupling.

To reproduce the data in Fig. 2(b), we introduce the linewidths as the imaginary parts of the resonance fields in Eq. (1):
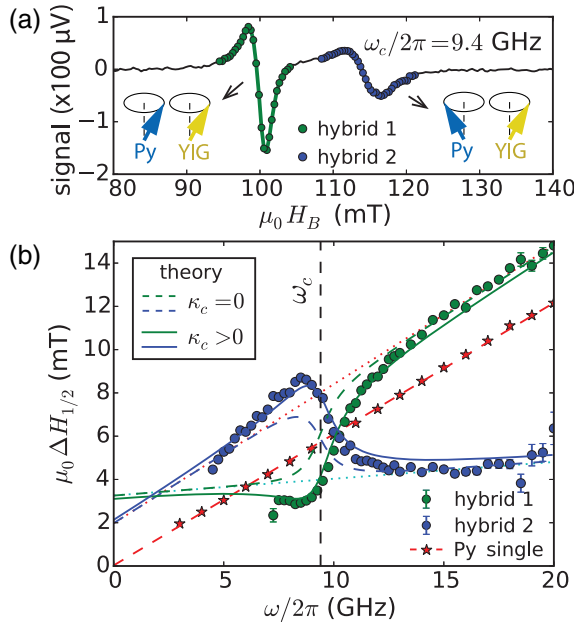

FIG. 2. (a) The line shape of the YIG(100 nm)/Py(7.5 nm) sample at $\omega_c/2\pi = 9.4$ GHz, showing different linewidths between the two hybrid modes of YIG($n = 2$) and Py($n = 0$) resonances. (b) Linewidths of the two hybrid modes as a function of frequency. Dotted lines show the linear fit of the linewidths for the two uncoupled modes. Dashed curves show the theoretical values with $\kappa_c = 0$. Solid curves show the fits with finite κ_c.

$$\mu_0(H_c^\pm + i\Delta H_{1/2}^\pm)$$
$$= \mu_0\frac{H_r^{\mathrm{YIG}} + H_r^{\mathrm{Py}}}{2} + i\mu_0\frac{\kappa_{\mathrm{YIG}} + \kappa_{\mathrm{Py}}}{2}$$
$$\pm \sqrt{\left(\mu_0\frac{H_r^{\mathrm{YIG}} - H_r^{\mathrm{Py}}}{2} + i\mu_0\frac{\kappa_{\mathrm{YIG}} - \kappa_{\mathrm{Py}}}{2}\right)^2 + \tilde{g}_c^2}, \quad (2)$$

where $\kappa_{\mathrm{YIG(Py)}}$ is the uncoupled linewidth of YIG (Py) from the linear extraction (dotted lines) in Fig. 2(b), and $\tilde{g}_c = g_c + i\kappa_c$ is the complex interfacial coupling strength with an additional dampinglike component κ_c from spin pumping. In order to show the relationship between the spin pumping from the coherent YIG-Py dynamics and the *incoherent* spin pumping from the individual Py dynamics, we identify the latter as the linewidth enhancement of Py(7.5 nm), $\Delta H_{\mathrm{sp}}^{\mathrm{Py}}$, between the linearly extrapolated YIG/Py [red dots in Fig. 2(b)] and Si/SiO_2/Py [red stars in Fig. 2(b)]. Then, we quantify the coherent dampinglike coupling strength κ_c as $\kappa_c(\omega) = \beta\mu_0\Delta H_{\mathrm{sp}}^{\mathrm{Py}}(\omega)$, where β is a unitless and frequency-independent value measuring the ratio between the coherent and incoherent spin pumping. For the best fit value, $\beta = 0.82$, Eq. (2) nicely reproduces the data in Fig. 2(b). For comparison, if we set $\kappa_c(\omega) = 0$ in Eq. (2), we obtain the blue and green dashed curves, which result in identical linewidth at ω_c as opposed to the data in Fig. 2(a).

In order to understand the physical meaning of $\tilde{g}_c$, we consider the coupled LLG equations of the YIG/Py bilayer [26,32,34] in the macrospin limit:

$$\frac{d\mathbf{m}_i}{dt} = -\mu_0\gamma_i\mathbf{m}_i \times \mathbf{H}_{\mathrm{eff}} + \alpha_i\mathbf{m}_i \times \frac{d\mathbf{m}_i}{dt} - \gamma_i\mathbf{m}_i \times \frac{J}{M_i t_i}\mathbf{m}_j$$
$$+ \Delta\alpha_i\left(\mathbf{m}_i \times \frac{d\mathbf{m}_i}{dt} - \mathbf{m}_j \times \frac{d\mathbf{m}_j}{dt}\right), \quad (3)$$

where $\mathbf{m}_{i,j}$ is the unit magnetization vector, $\mathbf{H}_{\mathrm{eff}}$ is the effective field including H_B, H_{ex}, and the demagnetizing field, and α_i is the intrinsic Gilbert damping. The index is defined as $(i, j) = (1, 2)$ or $(2,1)$. In the last two coupling terms, J is the interfacial exchange energy and $\Delta\alpha_i = \gamma_i\hbar g^{\uparrow\downarrow}/(4\pi M_i t_i)$ is the spin pumping damping enhancement with $g^{\uparrow\downarrow}$ the spin mixing conductance. The two terms provide the fieldlike and dampinglike coupling torques, respectively, between $\mathbf{m}_i$ and $\mathbf{m}_j$. To view the dampinglike coupling on a similar footing, we define its coupling energy J' as

$$J'(\omega) = \frac{g^{\uparrow\downarrow}}{4\pi}\hbar\omega. \quad (4)$$

Here J' describes the number of quantum channels per unit area ($g^{\uparrow\downarrow}$) for magnons ($\hbar\omega$) to pass through [31,34]; similarly, J describes the number and strength of exchange bonds between YIG and Py per unit area. From the definition, we can express the spin pumping linewidth

enhancement as $\mu_0 \Delta H_{sp}^i(\omega) = J'(\omega)/M_i t_i$, in pair with the exchange field term in Eq. (3). By solving Eq. (3) we find

$$\kappa_i(\omega) = \frac{\alpha_i \omega}{\gamma_i} + \frac{J'(\omega)}{M_i t_i}, \tag{5a}$$

$$g_c = f(\omega_c)\sqrt{\frac{J}{M_1 t_1}\frac{J}{M_2 t_2}}, \tag{5b}$$

$$\kappa_c(\omega_c) = f(\omega_c)\sqrt{\frac{J'(\omega_c)}{M_1 t_1}\frac{J'(\omega_c)}{M_2 t_2}}, \tag{5c}$$

with the dimensionless factor $f(\omega)$ accounting for the precession elliptical asymmetry. $f(\omega) = 1$ for identical ellipticity ($M_1 = M_2$) and $f(\omega_c) = 0.9$ in the case of YIG and Py; see the Supplemental Material for details [45]. Equation (5) shows that both g_c and $\kappa_c(\omega_c)$ are proportional to $1/\sqrt{t_i}$, which comes from the geometric averaging of the coupled magnetization dynamics. This is in contrast to the $1/t_i$ dependence of the uncoupled exchange field and spin pumping damping enhancement for a single layer, as shown in Eq. (5a). In Fig. 3(a), a good fitting of g_c to $1/\sqrt{t_{Py}}$ rather than $1/t_{Py}$ validates the model. In the limit of zero Py thickness, the model breaks down due to the significance of boundary pinning and the assumption of macrospin dynamics, as reflected in the reduction of g_c at $t_{Py} = 5$ nm.

For the dampinglike coupling, we plot β instead as a function of t_{Py} in order to minimize the variation in the quality of interfacial coupling and the frequency dependence of $\kappa_c(\omega_c)$. By taking the ratio between $\kappa_c(\omega_c)$ and $\mu_0 \Delta H_{sp}^{Py}(\omega_c)$ from the analytical model, we obtain the macrospin expression $\beta = f(\omega_c)\sqrt{M_{Py} t_{Py}/M_{YIG} t_{YIG}}$ with $f(\omega_c) = 0.9$. Figure 3(b) shows that the extracted β^2 varies linearly with t_{Py}, rather than being independent of it as
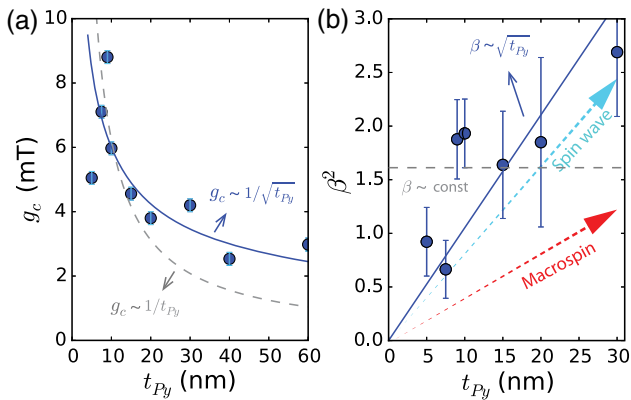
would be expected for incoherent spin pumping. The fit is not perfect, which may be caused by (i) the variation of inhomogeneous broadening of Py in YIG/Py bilayers or (ii) the multipeak line shapes in YIG [see YIG $n = 0$ line shapes in Fig. 1(b)] due to possible damage during the ion milling process.

If we calculate β from the macrospin approximation, the prediction, shown in the red dashed arrow in Fig. 3(b), differs significantly from the experimental data. To account for the difference, we consider a spin wave model for the YIG/Py bilayer, where finite wave numbers exist in both layers and are determined from the boundary condition [46]. For simplicity, we consider free pinning at the two exterior surfaces of YIG and Py and Hoffmann exchange boundary conditions for the interior interface of YIG/Py [47]. From the spin wave model, we find an additional factor of $\sqrt{2}$ in Eqs. (5b) and (5c); see the Supplemental Material for details [45]. This factor arises because the nonuniform profile of the PSSW mode in YIG reduces the effective mode volume by a factor of 2 compared with the uniform mode. A similar effect has been previously discussed in spin pumping from PSSW modes [48,49]. In Fig. 3(b) the theoretical calculation from the spin wave model (cyan dashed arrow) is close to the experimental values. This is an additional evidence of the coherent spin pumping in YIG/Py bilayers.

Figure 4 compares the values of J and J' obtained from the hybrid dynamics. For convenience we estimate the value of J' from Eq. (5c), as $J'(\omega_c) = \kappa_c(\omega_c)/f(\omega_c)\sqrt{M_{YIG} t_{YIG} M_{Py} t_{Py}/2}$. Noting the frequency

FIG. 3. (a) Extracted g_c as a function of t_{Py}. (b) Extracted β^2 as a function of t_{Py}. In both panels, the solid and dashed curves are the fits of data to the coherent and incoherent models, respectively. In (b), the red and cyan dotted arrows show the theoretical predictions for the coherent models based on the macrospin and spin wave approximations, respectively. Error bars indicate single standard deviations found from the fits to the line shape.
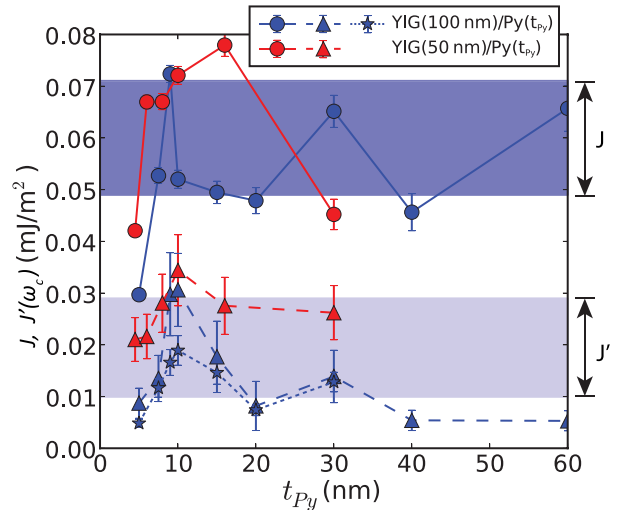

FIG. 4. Thickness dependence of J (circles) and $J'(\omega_c)$ (triangles), which are calculated from g_c and $\kappa_c(\omega_c)$, respectively. Blue points denote the results for YIG(100 nm)/Py(t_{Py}) and red points for YIG(50 nm)/Py(t_{Py}). The blue stars denote $J'_{sp}(\omega_c)$, in which $\Delta H_{sp}^{Py}(\omega_c)$ is calculated from the Py linewidth enhancement from Py(t_{Py}) to YIG(100 nm)/Py(t_{Py}). Error bars indicate single standard deviations found from the fits to the line shape.

TABLE I. Fieldlike, dampinglike coupling energy and spin mixing conductance for the YIG/Py interface. The value of J' is calculated around $\omega_c/2\pi = 9$ GHz.

	J (mJ/m^2)	J' (mJ/m^2)	$g^{\uparrow\downarrow}$ (nm^{-2})
YIG/Py	0.060 ± 0.011	0.019 ± 0.009	42 ± 21

dependence of $J'(\omega)$, all the values of $J'(\omega)$ in this work are obtained around $\omega_c/2\pi = 9$ GHz. We can also calculate $J'(\omega_c)$ from the uncoupled spin pumping effect, as $J'_{\rm sp}(\omega_c) = \mu_0 \Delta H^{\rm Py}_{\rm sp}(\omega_c) M_{\rm Py} t_{\rm Py}$. For the YIG/Py interface, the value of J stays at the same level; the value of $J'(\omega_c)$ fluctuates with samples but is well aligned with $J'_{\rm sp}(\omega_c)$, which again supports that the dampinglike interfacial coupling comes from spin pumping. Furthermore, we have also repeated the experiments for a thinner YIG(50 nm)/Py(t) sample series and obtained similar values of J and $J'(\omega_c)$, as shown in Fig. 4.

Table I summarizes the values of J, J', and $g^{\uparrow\downarrow}$ for the YIG/Py interface, where J' is taken from the vicinity of $\omega_c/2\pi = 9$ GHz and $g^{\uparrow\downarrow}$ is calculated from $J'(\omega_c)$ by Eq. (4). The value of J is much smaller than a perfect exchange-coupled interface, which is not surprising given the complicated and uncharacterized nature of the YIG/Py interface. For Py, the interfacial exchange energy can be estimated [46] by $2A_{\rm ex}/a$, where for Py $A_{\rm ex} = 12$ pJ/m [49] and the lattice parameter $a = 0.36$ nm. We find $2A_{\rm ex}/a = 68$ mJ/m^2, 3 orders of magnitude larger than J. Comparing with similar interfaces, our reported J is similar to YIG/Ni (0.03 mJ/m^2 [27]) and smaller than YIG/Co (0.4 mJ/m^2 [26]). A different interlayer exchange coupling from Ruderman-Kittel-Kasuya-Yosida interaction may generate a larger J [50–52] but a smaller $g^{\uparrow\downarrow}$ [53]. There could also be a fieldlike contribution of J from $g^{\uparrow\downarrow}$ [23,26,54–56]. But since the exchange J dominates in the coupled dynamics, it is difficult to distinguish the spin mixing conductance contribution in our experiments.

In conclusion, we have characterized the dampinglike coupling torque between two exchange-coupled ferromagnetic thin films. By exciting the hybrid dynamics in the strong-coupling regime, this dampinglike torque can either increase or suppress the total damping in the out-of-phase or in-phase mode, respectively. The origin of the dampinglike torque is the coherent spin pumping from the coupling magnetization dynamics. Our results reveal new insight for tuning the coherence in magnon-magnon hybrid dynamics and are important for magnon-based coherent information processing.

*web54@columbia.edu
†weizhang@oakland.edu
‡Current address: Department of Materials Science and Engineering, University of Illinois at Urbana-Champaign, Urbana, IL 61801, USA.
axelh@illinois.edu

[1] M. H. Devoret and R. J. Schoelkopf, Science **339,** 1169 (2013).
[2] D. D. Awschalom, L. C. Bassett, A. S. Dzurak, E. L. Hu, and J. R. Petta, Science **339,** 1174 (2013).
[3] F. J. Dyson, Phys. Rev. **102,** 1217 (1956).
[4] A. V. Chumak, V. I. Vasyuchka, A. A. Serga, and B. Hillebrands, Nat. Phys. **11,** 453 (2015).
[5] A. Khitun, M. Bao, and K. L. Wang, IEEE Trans. Magn. **44,** 2141 (2008).
[6] T. Schneider, A. A. Serga, B. Leven, B. Hillebrands, R. L. Stamps, and M. P. Kostylev, Appl. Phys. Lett. **92,** 022505 (2008).
[7] V. V. Kruglyak, S. O. Demokritov, and D. Grundler, J. Phys. D **43,** 264001 (2010).
[8] S. Kaka, M. R. Pufall, W. H. Rippard, T. J. Silva, S. E. Russek, and J. A. Katine, Nature (London) **437,** 389 (2005).
[9] F. B. Mancoff, N. D. Rizzo, B. N. Engel, and S. Tehrani, Nature (London) **437,** 393 (2005).
[10] N. Locatelli, A. Hamadeh, F. A. Araujo, A. D. Belanovsky, P. N. Skirdkov, R. Lebrun, V. V. Naletov, K. A. Zvezdin, M. Muñoz, J. Grollier, O. Klein, V. Cros, and G. de Loubens, Sci. Rep. **5,** 17039 (2015).
[11] Y. Li, X. de Milly, F. A. Araujo, O. Klein, V. Cros, J. Grollier, and G. de Loubens, Phys. Rev. Lett. **118,** 247202 (2017).
[12] R. Lebrun, S. Tsunegi, P. Bortolotti, H. Kubota, A. S. Jenkins, M. Romera, K. Yakushiji, A. Fukushima, J. Grollier, S. Yuasa, and V. Cros, Nat. Commun. **8,** 15825 (2017).
[13] A. Awad, P. D:urrenfeld, A. Houshang, M. Dvornik, E. Iacocca, R. K. Dumas, and J. Åkerman, Nat. Phys. **13,** 292 (2017).
[14] D. Vodenicarevic, N. Locatelli, F. Abreu Araujo, J. Grollier, and D. Querlioz, Sci. Rep. **7,** 44772 (2017).
[15] M. Romera, P. Talatchian, S. Tsunegi, F. Abreu Araujo, V. Cros, P. Bortolotti, J. Trastoy, K. Yakushiji, A. Fukushima, H. Kubota, S.. Yuasa, M. Ernoult, D. Vodenicarevic, T. Hirtzlin, N. Locatelli, D. Querlioz, and J. Grollier, Nature (London) **563,** 230 (2018).
[16] H. Huebl, C. W. Zollitsch, J. Lotze, F. Hocke, M. Greifenstein, A. Marx, R. Gross, and S. T. B. Goennenwein, Phys. Rev. Lett. **111,** 127003 (2013).

[17] Y. Tabuchi, S. Ishino, T. Ishikawa, R. Yamazaki, K. Usami, and Y. Nakamura, Phys. Rev. Lett. **113**, 083603 (2014).

[18] X. Zhang, C.-L. Zou, L. Jiang, and H. X. Tang, Phys. Rev. Lett. **113**, 156401 (2014).

[19] M. Goryachev, W. G. Farr, D. L. Creedon, Y. Fan, M. Kostylev, and M. E. Tobar, Phys. Rev. Applied **2**, 054002 (2014).

[20] L. Bai, M. Harder, Y. P. Chen, X. Fan, J. Q. Xiao, and C.-M. Hu, Phys. Rev. Lett. **114**, 227201 (2015).

[21] Y. Li, T. Polakovic, Y.-L. Wang, J. Xu, S. Lendinez, Z. Zhang, J. Ding, T. Khaire, H. Saglam, R. Divan, J. Pearson, W.-K. Kwok, Z. Xiao, V. Novosad, A. Hoffmann, and W. Zhang, Phys. Rev. Lett. **123**, 107701 (2019).

[22] J. T. Hou and L. Liu, Phys. Rev. Lett. **123**, 107702 (2019).

[23] L. McKenzie-Sell, J. Xie, C.-M. Lee, J. W. A. Robinson, C. Ciccarelli, and J. A. Haigh, Phys. Rev. B **99**, 140414(R) (2019).

[24] Y. Tabuchi, S. Ishino, A. Noguchi, T. Ishikawa, R. Yamazaki, K. Usami, and Y. Nakamura, Science **349**, 405 (2015).

[25] D. Lachance-Quirion, Y. Tabuchi, S. Ishino, A. Noguchi, T. Ishikawa, R. Yamazaki, and Y. Nakamura, Sci. Adv. **3**, e1603150 (2017).

[26] S. Klingler, V. Amin, S. Geprägs, K. Ganzhorn, H. Maier-Flaig, M. Althammer, H. Huebl, R. Gross, R. D. McMichael, M. D. Stiles, S. T. B. Goennenwein, and M. Weiler, Phys. Rev. Lett. **120**, 127201 (2018).

[27] J. Chen, C. Liu, T. Liu, Y. Xiao, K. Xia, G. E. W. Bauer, M. Wu, and H. Yu, Phys. Rev. Lett. **120**, 217202 (2018).

[28] H. Qin, S. J. Hämäläinen, and S. van Dijken, Sci. Rep. **8**, 5755 (2018).

[29] C. Liu, J. Chen, T. Liu, F. Heimbach, H. Yu, Y. Xiao, J. Hu, M. Liu, H. Chang, T. Stueckler, S. Tu, Y. Zhang, Y. Zhang, P. Gao, Z. Liao, D. Yu, K. Xia, N. Lei, W. Zhao, and M. Wu, Nat. Commun. **9**, 738 (2018).

[30] K. An, V. S. Bhat, M. Mruczkiewicz, C. Dubs, and D. Grundler, Phys. Rev. Applied **11**, 034065 (2019).

[31] Y. Tserkovnyak, A. Brataas, and G. E. W. Bauer, Phys. Rev. Lett. **88**, 117601 (2002).

[32] B. Heinrich, Y. Tserkovnyak, G. Woltersdorf, A. Brataas, R. Urban, and G. E. W. Bauer, Phys. Rev. Lett. **90**, 187601 (2003).

[33] K. Lenz, T. Toliński, J. Lindner, E. Kosubek, and K. Baberschke, Phys. Rev. B **69**, 144422 (2004).

[34] Y. Tserkovnyak, A. Brataas, G. E. W. Bauer, and B. I. Halperin, Rev. Mod. Phys. **77**, 1375 (2005).

[35] S. S.-L. Zhang and S. Zhang, Phys. Rev. B **86**, 214424 (2012).

[36] V. P. Amin, J. Zemen, and M. D. Stiles, Phys. Rev. Lett. **121**, 136805 (2018).

[37] Y. S. Chen, J. G. Lin, S. Y. Huang, and C. L. Chien, Phys. Rev. B **99**, 220402(R) (2019).

[38] B. F. Miao, S. Y. Huang, D. Qu, and C. L. Chien, Phys. Rev. Lett. **111**, 066602 (2013).

[39] P. Hyde, L. Bai, D. M. J. Kumar, B. W. Southern, C.-M. Hu, S. Y. Huang, B. F. Miao, and C. L. Chien, Phys. Rev. B **89**, 180404(R) (2014).

[40] S. Li, W. Zhang, J. Ding, J. E. Pearson, V. Novosad, and A. Hoffmann, Nanoscale **8**, 388 (2016).

[41] M. B. Jungfleisch, V. Lauer, R. Neb, A. V. Chumak, and B. Hillebrands, Appl. Phys. Lett. **103**, 022411 (2013).

[42] C. Kittel, Phys. Rev. **73**, 155 (1948).

[43] C. Herring and C. Kittel, Phys. Rev. **81**, 869 (1951).

[44] S. Klingler, A. V. Chumak, T. Mewes, B. Khodadadi, C. Mewes, C. Dubs, O. Surzhenko, B. Hillebrands, and A. Conca, J. Phys. D **48**, 015001 (2014).

[45] See Supplemental Material at http://link.aps.org/supplemental/10.1103/PhysRevLett.124.117202 for details.

[46] B. Hillebrands, Phys. Rev. B **41**, 530 (1990).

[47] F. Hoffmann, A. Stankoff, and H. Pascard, J. Appl. Phys. **41**, 1022 (1970).

[48] A. Kapelrud and A. Brataas, Phys. Rev. Lett. **111**, 097602 (2013).

[49] Y. Li and W. E. Bailey, Phys. Rev. Lett. **116**, 117602 (2016).

[50] S. S. P. Parkin, N. More, and K. P. Roche, Phys. Rev. Lett. **64**, 2304 (1990).

[51] M. Belmeguenai, T. Martin, G. Woltersdorf, M. Maier, and G. Bayreuther, Phys. Rev. B **76**, 104414 (2007).

[52] L. Fallarino, V. Sluka, B. Kardasz, M. Pinarbasi, A. Berger, and A. D. Kent, Appl. Phys. Lett. **109**, 082401 (2016).

[53] H. Yang, Y. Li, and W. E. Bailey, Appl. Phys. Lett. **108**, 242404 (2016).

[54] J. Sklenar, W. Zhang, M. B. Jungfleisch, W. Jiang, H. Chang, J. E. Pearson, M. Wu, J. B. Ketterson, and A. Hoffmann, Phys. Rev. B **92**, 174406 (2015).

[55] T. Nan, S. Emori, C. T. Boone, X. Wang, T. M. Oxholm, J. G. Jones, B. M. Howe, G. J. Brown, and N. X. Sun, Phys. Rev. B **91**, 214416 (2015).

[56] L. Zhu, D. C. Ralph, and R. A. Buhrman, Phys. Rev. Lett. **123**, 057203 (2019).

[57] L. McKenzie-Sell, J. Xie, C.-M. Lee, J. W. A. Robinson, C. Ciccarelli, and J. A. Haigh, Phys. Rev. B **99**, 140414(R) (2019).